Journal of
Materials Chemistry C

ROYAL SOCIETY OF CHEMISTRY

PAPER

View Article Online
View Journal | View Issue

Cite this: *J. Mater. Chem. C*, 2019, 7, 10642

Laser-induced photoresistance effect in Si-based vertical standing MoS_2 nanoplate heterojunctions for self-powered high performance broadband photodetection

Shuang Qiao,[abc] Jihong Liu,*[a] Guangsheng Fu,[a] Shufang Wang,*[a] Kailiang Ren*[bc] and Caofeng Pan*[bc]

Received 27th June 2019,
Accepted 2nd August 2019

DOI: 10.1039/c9tc03454d

rsc.li/materials-c

MoS_2 has attracted extensive attention as the basic configuration of optoelectronic systems because of its outstanding optical and electronic properties. Although high performance MoS_2-based photodetectors have been realized by many groups, these studies are still in their initial stages of research, and more importantly, the usual photocurrent or photovoltage signals are fundamentally susceptible, thus seeking novel structures or working principle devices becomes more fascinating. Here, the MoS_2/Si heterojunction is prepared with a vertically standing nanoplate structure and we exploit it as a photovoltage, photocurrent and photoresistance-based multifunctional self-powered position sensitive detector (PSD). The PSD exhibits unprecedented performance with very high sensitivity (391.1 mV mm^{-1}, 285.2 μA mm^{-1}, and 21.61 KΩ mm^{-1} for photovoltage, photocurrent and photoresistance responses, respectively), excellent linearity (nonlinearity $<2\%$), and a very fast response speed (4.75 ms/6.33 ms), all of which are much better than those obtained in many other systems. More importantly, it is the first time that lateral photoresistance (LPRE) is observed in a MoS_2/Si heterojunction. Based on the theoretical analysis of the scattering or transportation modulation of photo-generated carriers on the drifted carriers in the MoS_2/Si heterojunction, these results are well explained.

1. Introduction

Transition metal dichalcogenides (TMDs), as typical two dimensional (2D) layered nanomaterials, have aroused increasing interest due to the outstanding optical, electrical, photoelectric, and piezo-phototronic properties as well as easy compatibility with other 2D or 3D nanomaterials for constructing various functional heterostructures.[1–6] Among these TMDs, molybdenum disulfide (MoS_2) stands out in view of its high carrier mobility, tunable energy band-gap, large light absorptivity, and very excellent environmental stability.[7–10] More importantly, to date, many different MoS_2-based heterostructures have been prepared and successfully developed into field-effect transistors,[7,11] photodetectors,[12,13] photocatalysts,[14,15] gas sensors,[16,17] and photovoltaic devices,[6,18] and have been demonstrated to exhibit very brilliant properties, such as substantial on/off current ratio ($\sim10^8$),[7] large photoresponsivity ($\sim10^6$ A W^{-1}),[19] high detectivity ($\sim10^{14}$ Jones),[20] ultrafast response speed ($\sim$5 ns),[21] and great power conversion efficiency ($\sim$13.3%).[22] These fantastic and unique features have increasingly made MoS_2 one of the optimum candidates for exploiting multifunctional optoelectronic devices. Recently, the MoS_2-based photodetector, as a key component of optoelectronic systems, has been extensively investigated[7,11–13,19,23,24] because of the urgent need for highly sensitive and ultrafast photodetection, *e.g.* optical communications,[25] imaging,[26] environmental monitoring,[27] and position detection.[28] However, these studies are still in their initial stages and the experimental devices are far from practical applications. For both researchers and producers, high detection sensitivity or responsivity has always been an everlasting goal. The fundamental reason may be mainly attributed to two aspects, one is to reduce the power consumption; the other is to get a stable and credible signal. Therefore, self-powered devices have been developed and have gained a great reputation.[4,29] While, to improve the device performances and detection capabilities, many different methods have been tried, such as modulating layer thickness,[13] stacking with other 2D materials,[30,31] designing and optimizing the architecture of MoS_2,[24,32] external field modulation,[23,33,34] and even combining

[a] *Hebei Key Laboratory of Optic-Electronic Information and Materials, National & Local Joint Engineering Laboratory of New Energy Photoelectric Devices, College of Physics Science and Technology, Hebei University, Baoding 071002, P. R. China. E-mail: liujihong@hbu.edu.cn, sfwang@hbu.edu.cn*
[b] *Beijing Institute of Nanoenergy and Nanosystems, Chinese Academy of Sciences, Beijing, 100083, China. E-mail: renkailiang@binn.cas.cn, cfpan@binn.cas.cn*
[c] *CAS Center for Excellence in Nanoscience, National Center for Nanoscience and Technology (NCNST), Beijing, 100190, P. R. China*

Published on 02 August 2019. Downloaded by Beijing Institute of Nanoenergy and Nanosystems CAS on 9/4/2019 3:00:41 PM.

This journal is © The Royal Society of Chemistry 2019

Published on 02 August 2019. Downloaded by Beijing Institute of Nanoenergy and Nanosystems CAS on 9/4/2019 3:00:41 PM.

with the traditional semiconductors.[20,21,35,36] However, there are still unsolved issues in the measurement accuracy and stability even though very high photocurrent or photovoltage responses have been realized as these signals are usually easily affected by the operating circuits or working conditions due to their fundamentally susceptible characteristics. In contrast, besides current and voltage responses, there is another parameter of resistance deserving to be developed. More importantly, resistance derives from the scattering of lattice and electrons, and presents an intrinsic property of a material, thus seeking resistance-modulated devices has always been a great pursuit for scientists and engineers. To date, several different methods have already been successfully used to control or modulate the resistance,[37–40] and some devices have even been commercialized and are used in our daily lives, *e.g.* magnetoresistance hard disk and superconductivity, but photo-modulated resistance detectors have been seldomly reported, especially in MoS_2-based heterojunctions, and their photoresistance responses and the related working mechanisms are still unclear.

In this paper, the MoS_2 nanoplates were prepared on a p-doped Si substrate with a vertically standing structure to form a very good p–n heterojunction. Firstly, the lateral photovoltaic effect (LPVE), as well as the lateral photocurrent effect (LPCE), was studied in the MoS_2/Si heterojunction. This heterojunction exhibits outstanding lateral photovoltage and photocurrent responses in a broadband wavelength range with photovoltage and photocurrent responses up to 391.1 mV mm^{-1} and 285.2 μA mm^{-1}, and nonlinearity of no more than ~2% and ~1% (very good linearity), respectively, and especially without adding any external power, demonstrating its promising prospect in a self-powered light position sensitive detector (PSD). More importantly, considering the carrier gradient principle of LPVE or LPCE in the irradiated and non-irradiated regions of the MoS_2 layer, it is suggested that this mechanism can also be used to regularly modulate the layer resistance by changing the intrinsic scattering or transportation of the carriers, thus developing this heterojunction into a photoresistance-based PSD, which can be called a lateral photoresistance effect (LPRE). The LPRE results demonstrate that the surface layer resistance of the MoS_2/Si heterojunction exhibits a linear relationship with the laser position, and the photoresistance response increases gradually with both increasing laser power and decreasing external bias voltage with a maximum sensitivity of up to ~21.61 KΩ mm^{-1}. However, there is a threshold power (or voltage), above (or below) which the laser position-dependent photoresistance curve tends to be nonlinear, and the threshold voltage increases with enhancing the laser power. These results can be well understood based on the scattering or transportation modulation of photogenerated carriers on the drift carriers (electrons) in the MoS_2 layer of the heterojunction. Besides, it is found that the LPRE of this heterojunction has a broadband response range (at least 405 to 980 nm) and exhibits a very fast response speed (4.75 ms/6.33 ms). Our work provides an essential insight into the implementation of high-performance and novel photoelectric devices based on the photoresistance effect.

2. Experimental methods

The vertically standing MoS_2 nanoplates were prepared on the p-doped Si (with thickness of ~500 μm) substrate by using magnetron sputtering. The resistivity of the Si substrate was ~10 Ω cm (room temperature), and a 1.2 nm-thick native SiO_2 layer was produced on the surface. Prior to the deposition, the wafer was carefully cleaned according to a standard cleaning technique to remove the ionic and organic impurities. During the preparation, a composite MoS_2 target (99.998%) was selected as the sputtering source and the chamber was evacuated to $\sim 1.0 \times 10^{-5}$ Pa at first, then the substrate temperature was increased to 500 °C and argon gas was bubbled by maintaining a 25 sccm flow rate and a 1.0 Pa pressure, and at last, the sputtering power of 50 W was added keeping a 2.0 nm min^{-1} deposition rate. Here, a 50 nm-thick vertical standing MoS_2 nanoplate layer was prepared, considering the best response at this thickness.[28] After the preparation, two strip electrodes of Ti/Au (5 nm\50 nm) were deposited on the top layer with a ~0.5 mm electrode width and a ~0.6 mm distance controlled by a metal mask, and a planar electrode of Ag (60 nm) was prepared on the Si substrate using the thermal evaporation technique.

The structure and the morphologies of the heterojunction were characterized by X-ray diffraction (XRD) and scanning electron microscopy (SEM), respectively. The optical properties were identified by Raman and UV spectroscopies. The *I–V* property was characterized using a Keithley SourceMeter (2400) and home-built equipment combining an SR570 current source, an SR560 voltage source, and continuous wave laser illumination. The LPVE, LPCE and LPRE were measured by using home-built equipment including a Keithley 2400 SourceMeter, a three-dimensional motorized linear stage, and several continuous-wave lasers with wavelengths of 405, 450, 532, 671, 808, and 980 nm, respectively. The response speed of the heterojunction was determined by using an SR570 current source, an SR560 voltage source, and a laser chopper.

3. Results and discussion

The surface and cross-sectional morphologies of the MoS_2 nanoplates and the heterojunction are identified by SEM, with the surface images of different magnification sizes shown in Fig. 1a and b, respectively, and the cross-sectional image shown in Fig. 1c (as the cross-sectional morphology is hard to observe for the thinner vertical standing MoS_2 nanoplates, we choose a 100 nm thick sample to well illustrate the structure). The MoS_2 film obviously shows a vertically standing nanoplate structure, and a distinct interface can be found between the Si substrate and the MoS_2 nanoplates. Fig. 1d shows the XRD result. Besides the Si(400) diffraction peak, two other relatively weak peaks at 13.1° and 33.5° can be observed, which can be indexed as the (002) and (100) diffraction peaks of the MoS_2 layer,[41] and the low diffraction intensity can be ascribed to the poor crystal quality. The Raman result of the heterojunction is given in Fig. 1e. Two characteristic MoS_2 vibration peaks are observed at 380.5 cm^{-1} and 408.2 cm^{-1},

Published on 02 August 2019. Downloaded by Beijing Institute of Nanoenergy and Nanosystems CAS on 9/4/2019 3:00:41 PM.

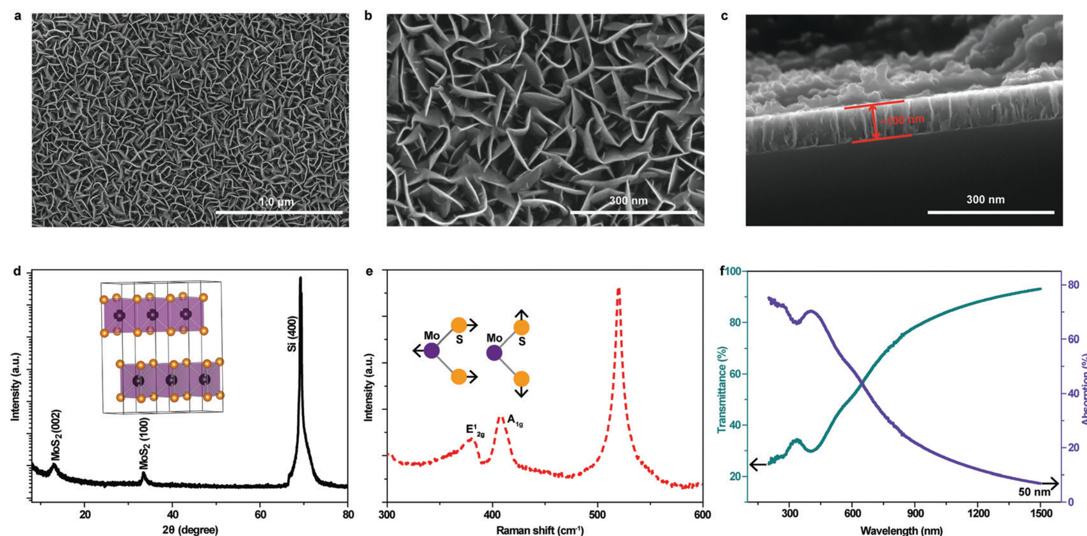

Fig. 1 The SEM surface morphology of the MoS_2 nanoplates in (a) large-scale, and (b) small-scale. (c) The SEM cross-sectional morphology of the MoS_2 nanoplates. The XRD diffraction (d) and the Raman (e) results of the heterojunction. (f) The absorption and transmission spectra of the MoS_2 layer on the glass sheet.

which represent the Mo atom and the S atom in-plane vibration mode (E^1_{2g}) and the S atom out-of-plane vibration mode (A_{1g}), respectively.[42] Fig. 1f gives the ultraviolet-visible spectrophotometer results of the 50 nm-thick vertical standing MoS_2 nanoplates prepared on glass sheets. The MoS_2 nanoplates exhibit a strong absorption and a wide spectral range, suggesting their great potential for high-performance broadband photoelectric devices.

Fig. 2a shows a schematic diagram of the lateral photoelectric research on the MoS_2/Si heterostructure. Before the measurements, the transverse current–voltage (*I–V*) curve is identified between the two top electrodes (Fig. 2b). The good linear behavior confirms the Ohmic relationship of the Ti/Au electrodes and the MoS_2 nanoplates, and meanwhile a constant resistance of $\sim$12390 Ω is deduced without depending on the bias voltage. To evaluate the photoresponse performances of the MoS_2/Si heterojunction, the longitudinal *I–V* curves are determined, as shown in Fig. 2c. A clear rectification feature can be observed in the dark, suggesting that a good p–n heterojunction

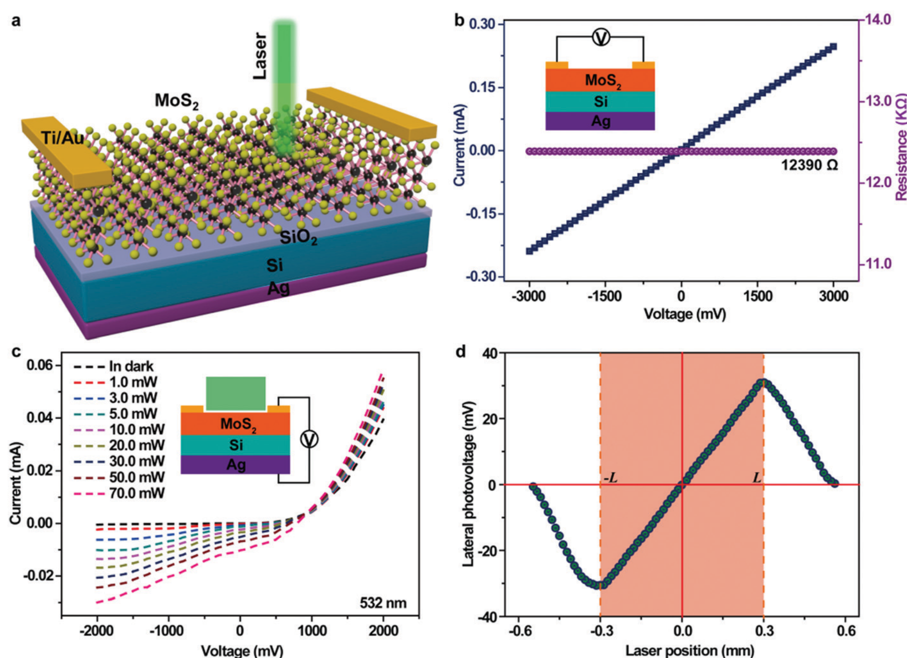

Fig. 2 (a) Schematic illustration of the lateral photoelectric effect in the MoS_2/Si heterojunction. (b) Transverse *I–V* result of the heterojunction and the surface layer resistance (with inset giving the measurement diagram). (c) Longitudinal *I–V* results of the device under illumination of different powers (with inset giving the measurement diagram). (d) A typical LPV curve of the heterojunction as a function of laser position.

 This journal is © The Royal Society of Chemistry 2019

Published on 02 August 2019. Downloaded by Beijing Institute of Nanoenergy and Nanosystems CAS on 9/4/2019 3:00:41 PM.

is formed. More importantly, the photocurrent response increases quickly with enhancing laser intensity even to ~70 mW under a 532 nm-laser illumination. Fig. 2d gives a typical laser position-dependent lateral photovoltage (LPV) curve of the heterojunction. With the laser beam moving from the left electrode (−L) to the right electrode (L), a linear relationship between the laser position and the LPV is found, demonstrating its enormous potential application in light PSD.

For the lateral photoelectric effect, it can be easily understood that when a laser beam is perpendicularly illuminated on the MoS_2 nanoplates, the energy could be absorbed by the Si substrate or the MoS_2 nanoplates and excite electron–hole pairs there. These generated carriers are separated by the built-in field and transmitted away (resulting in electrons entering into the top MoS_2 and holes entering into the bottom Si), and then the accumulated electrons around the laser beam would diffuse from the illuminated region to non-illuminated regions due to the density gradient in the MoS_2 nanoplates, leading to the different number of electrons collected by the two electrodes; thus, a lateral photovoltage (LPV) can be obtained when measured with a voltmeter between the two Ti/Au electrodes, called the LPVE (shown in Fig. 3a).[43,44] More importantly, there is no need for any external bias voltage in the LPVE, demonstrating its enormous promise for applications in self-powered photoelectric devices. Firstly, the LPVE is studied under illumination of different powers (changing from 0.3 mW to 70 mW, 1 mW corresponds to 12.7 W cm^{-2} laser density) with a 532 nm-laser, and the laser position-dependent LPV curves are given in Fig. 3b. The LPV response improves strongly with increasing laser power, which can be ascribed to the increased photogenerated carriers, as shown in Fig. 2c. To well illustrate it, a key parameter of position sensitivity is deduced by the linear fitting,[45] and it is usually better to get a larger position sensitivity for a device. The sensitivity increases largely from 146.6 mV mm^{-1} to 329.5 mV mm^{-1} with increasing power from 0.3 mW to 10 mW, and then increases gradually slowly to 391.1 mV mm^{-1} at 70 mW illumination, as shown in Fig. 3c. Ideally, the LPV is suggested to be linearly dependent on the laser position; however, there is more or less deviation in practice due to many different reasons,[46,47] and the nonlinearity should be no more than 15% for a qualified device.[45] Therefore, to judge the deviation of the LPV results, another key parameter of nonlinearity is proposed, which represents the deviation of the experimental result from the ideal linear curve and can be written as:[43,45]

$$\text{Nonlinearity}\ (\%) = \frac{2 \times \sqrt{\left[\sum_{i=1}^{N} \left(\text{LPV}_i - \text{LPV}_i^l\right)^2\right] \Big/ N}}{2L} \times 100\% \quad (1)$$

where N represents the number of the measured points, and LPV_i and LPV_i^l are the measured LPV and linearly fitted LPV value at the i point, respectively. Based on eqn (1), the nonlinearities are deduced and given in Fig. 3c(the inset). The LPV curves exhibit very excellent linearities with nonlinearity less than 2%, demonstrating the good quality and uniform layer structure of the heterojunction.

As shown in Fig. 3d, when changing the voltmeter to an amperemeter, a lateral photocurrent (LPC) can also be obtained, which is called the LPCE. The laser position-dependent LPC curves are measured under illumination of different laser powers of a 532 nm laser and summarized in Fig. 3e. The LPC response is also enhanced clearly with increasing laser power. Fig. 3f gives the extracted sensitivities of the photocurrents at different laser powers. The sensitivity increases gradually from 22.8 μA mm^{-1}

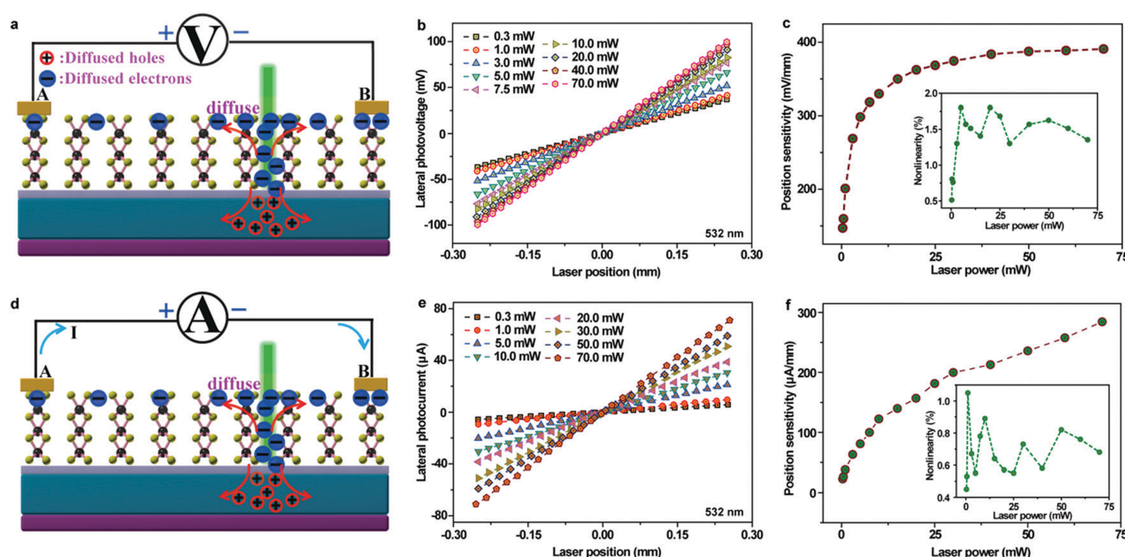

Fig. 3 (a) LPVE measurement diagram of the heterojunction. (b) The laser position-dependent LPV curves under illumination of different powers. (c) The extracted photovoltage sensitivities and nonlinearities (inset) of the LPV curves. (d) LPCE measurement diagram of the heterojunction. (e) The laser position-dependent LPC curves under illumination of different powers. (f) The extracted photocurrent sensitivities and nonlinearities (inset) of the LPC curves.

Published on 02 August 2019. Downloaded by Beijing Institute of Nanoenergy and Nanosystems CAS on 9/4/2019 3:00:41 PM.

to 285.2 μA mm^{-1}, which can be ascribed to the laser power-dependent photoelectric response of this heterojunction (as illustrated in Fig. 2c). Besides, the nonlinearities of the LPC curves are also very small (<1%), as shown in the inset of Fig. 3f. Based on the above results, it is notable that this heterojunction exhibits both very huge photovoltage and photocurrent sensitivities of 391.1 mV mm^{-1} and 285.2 μA mm^{-1}, respectively, the values of which are much larger than those obtained in most other systems.[46–51] Additionally, this heterojunction has an excellent lateral photoelectric response linearity and a considerable laser power working range, all of which could be attributed to the excellent capabilities of strong absorption, the quick longitudinal carrier transportation of the vertically standing MoS_2 nanoplates, and also the good quality of the heterojunction.

Considering the carrier gradient appearance of LPVE or LPCE in the illuminated and non-illuminated regions of the MoS_2 layer (Fig. 3a and d), it is suggested that this may also be used to regularly modulate the layer resistance by changing the intrinsic scattering or transportation of the carriers in the conductive layer, called the LPRE. The LPRE measurement sketch of the MoS_2/Si heterojunction is given in the inset of Fig. 4a. When an external voltage is applied to the two Ti/Au electrodes (acting as source and drain) in the dark, a constant drift electric current would flow from A (electrode) to B (electrode), and the movement of the drifting electrons would be accelerated or decelerated under laser beam illumination due to the enhanced or weakened scattering at the left side or right side of the laser beam, respectively;[40] thus, the resistance of the MoS_2 layer could be regularly modulated with the laser position changing from A to B gradually, and a laser position-dependent photoresistance curve is obtained. Fig. 4a and b show the lateral photoresistance (LPR) curves of a 0.2 V bias voltage under a 532 nm-laser illumination with power ranging from 0.3 mW to 30 mW and from 50 mW to 70 mW, respectively. It is obvious that the photoresistance response enhances with improving laser power, and the photoresistances are all linearly proportional to the laser position except the very large power illumination of 60 mW and 70 mW. On account of the linear relationship of the LPR and the laser position, this effect can also be used to develop photoresistance-modulated PSDs. Through the linear fitting and the nonlinearity calculation (eqn (1)), the photoresistance sensitivities and nonlinearities under illumination of different laser powers are deduced, as shown in Fig. 4c and d. Similar to the LPVE, the sensitivity increases quickly from 12.19 KΩ mm^{-1} to 21.48 KΩ mm^{-1} at first, and then tends to a nearly constant value of 21.61 KΩ mm^{-1} with increasing power from 0.3 mW to 50 mW, which can be attributed to the gradually enhanced scattering influence of the photogenerated carriers, as illustrated in Fig. 2c. However, the sensitivity increases greatly to 37.42 KΩ mm^{-1} with increasing laser power again (the shaded area in Fig. 4c). By comparing with the LPR results in Fig. 4b, the dramatic increment at very high laser powers should mainly result from the nonlinearly improved photoresistance. This can be directly demonstrated from the nonlinearity results as the nonlinearity fluctuates at around 1% in the low laser power regime (< ∼50 mW), and then deteriorates quickly from 2.1% to 14.3% with laser power increasing from 50 mW to 70 mW (the shaded area in Fig. 4d).

To identify the wavelength response of the LPRE in the heterojunction, the laser position-dependent LPR curves are

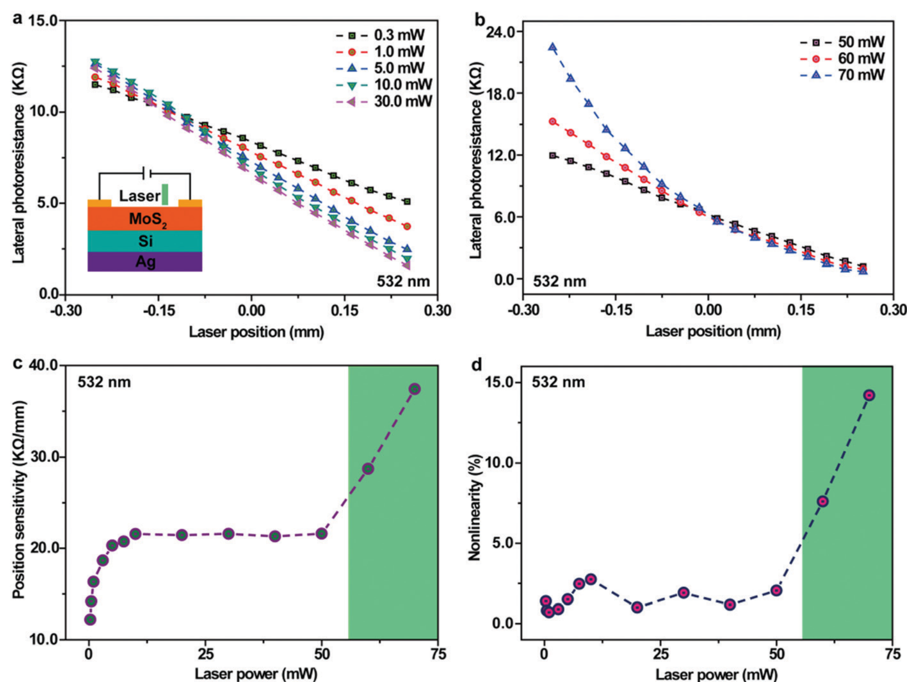

Fig. 4 The laser position-dependent LPR curves under illumination of different powers ranging from (a) 0.3 mW to 30 mW (with the inset giving the measurement diagram) and (b) 50 mW to 70 mW. The extracted (c) photoresistance sensitivities and (d) nonlinearities of the LPR curves.

This journal is © The Royal Society of Chemistry 2019

Published on 02 August 2019. Downloaded by Beijing Institute of Nanoenergy and Nanosystems CAS on 9/4/2019 3:00:41 PM.

determined under illumination of six different lasers (with wavelengths of 405, 450, 532, 671, 808, and 980 nm). The typical lateral photoresistance curves under illumination of 3 m W and applying a 0.2 V bias voltage are given in Fig. 5a. Obviously, this heterostructure has a broadband response range, and the lateral photoresistance curve still shows very excellent linearity (nonlinearity $<2\%$, as shown in Fig. 5b). However, the sensitivity, which enhances gradually (from 9.39 KΩ mm^{-1} to 19.71 KΩ mm^{-1}) with wavelength increasing from 405 to 671 nm, and then tends to reduce (from 19.71 KΩ mm^{-1} to 12.84 KΩ mm^{-1}) with wavelength increasing again even to 980 nm, exhibits a non-monotonic changing tendency, indicating the various photoexcited efficiencies of different lasers.

Then, the external voltage effect on the LPRE response is investigated. Fig. 5c presents the laser position-dependent lateral photoresistance curves measured under illumination of 3 mW (532 nm laser) and applying different bias voltages changing from 0.1 V to 5 V. The photoresistance curve shows a seriously nonlinear behavior when adding a bias voltage of 0.1 V (the nonlinearity is 14.2%, and the sensitivity reaches 41.57 KΩ mm^{-1}, as shown in Fig. 5d). However, the photoresistance starts to be linearly proportional to the laser position when the voltage exceeds $\sim$0.1 V, and the sensitivity decreases gradually (from 18.63 KΩ mm^{-1} to 7.35 KΩ mm^{-1}) with external voltage increasing from 0.2 V to 5 V (Fig. 5d). This is very similar to the results of changing laser power due to the relative scattering effect of the diffusion electrons on the drift electrons (increasing (or decreasing) the number of the diffusion electrons under illumination of large (or small) laser power is equivalent to decreasing (or increasing) the number of the drift electrons with applying low (or high) bias voltages). Moreover, it is observed that the averaged photoresistance increases a little with increasing external voltage, especially when the voltage reaches $\sim$10 V, the photoresistance is nearly independent of laser position again as that without laser illumination (as shown in the inset of Fig. 5c), which can be attributed to the negligible scattering effect of minority of diffusion electrons as compared with the majority of drift electrons.

To explain the physical mechanism of the LPRE and well understand the laser power- and bias voltage-dependent lateral photoresistance response and nonlinear behavior in the MoS_2/Si heterojunction, a theoretical model is proposed, as shown in Fig. 6a and b. When a laser beam illuminates the heterojunction, the laser energy can be absorbed by the MoS_2 nanoplates or the Si substrate, and then generates electron–hole pairs. According to the energy band diagram of the heterostructure in Fig. 6b, the electrons would be swept and tunneled to the MoS_2 side (and holes would be swept and tunneled to the Si side, correspondingly), resulting in excess electrons gathering in the illumination position, so that the electrons would diffuse around. In one dimensional approximation, the diffusion equation (steady-state) can be written as follows:[43,46]

$$D\frac{d^2N_\lambda(x)}{d^2x} = \frac{N_\lambda(x)}{\tau} \tag{2}$$

where D represents the diffusion coefficient, τ represents the carrier lifetime, and $N_\lambda(x)$ represents the electron distribution density at x position under illumination of a λ wavelength

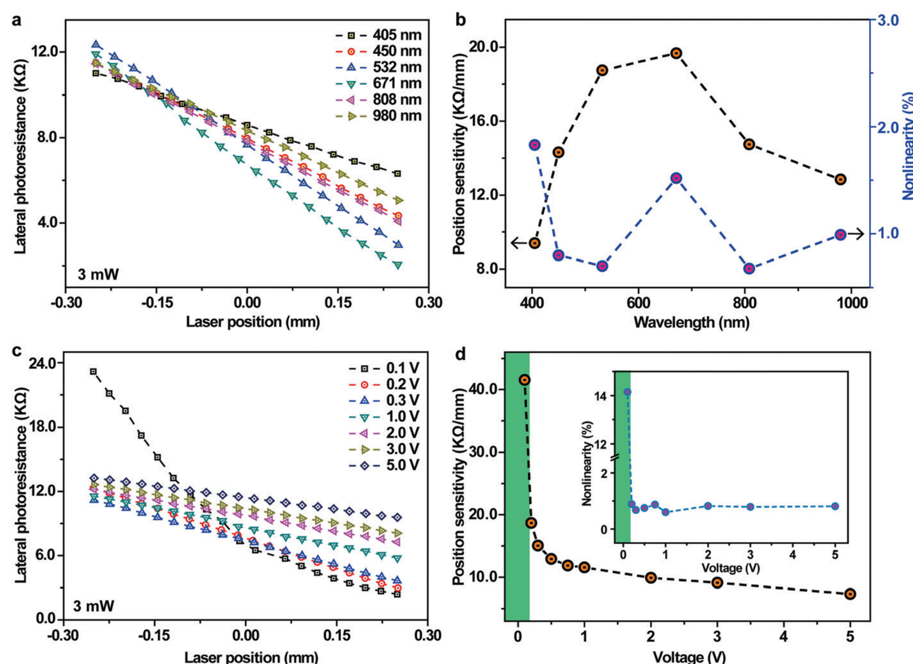

Fig. 5 (a) The laser position-dependent LPR curves under 3 mW illumination of different lasers. (b) The extracted wavelength-dependent position sensitivities and nonlinearities. (c) The laser position-dependent LPR curves under 3 mW illumination with adding different external voltages (with the inset giving the averaged resistance). (d) The extracted bias voltage-dependent position sensitivities and nonlinearities (inset).

View Article Online

Published on 02 August 2019. Downloaded by Beijing Institute of Nanoenergy and Nanosystems CAS on 9/4/2019 3:00:41 PM.

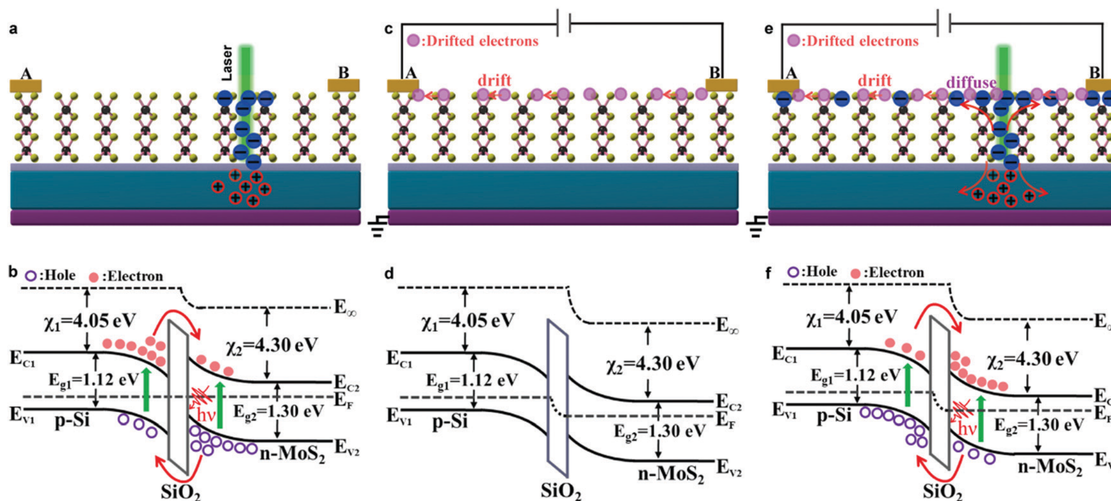

Fig. 6 (a, c and e) The working principle diagrams of the lateral photoelectric detector, the source–drain measurement and the LPRE detector. (b, d and f) The corresponding equilibrium energy band diagrams.

laser. From eqn (2), $N_\lambda(x)$ can be obtained:[43,46]

$$N_\lambda(x)=\begin{cases} N_\lambda(0)\exp\left(-\dfrac{x-x_0}{l_0}\right) & (x_0<x\le L)\\ N_\lambda(0)\exp\left(-\dfrac{x_0-x}{l_0}\right) & (-L\le x<x_0)\end{cases} \quad (3)$$

where x_0 represents the laser position, $N_\lambda(0)$ is the total electron density accumulated at x_0, and l_0 represents the carrier diffusion length. When a bias voltage is added on the two Ti/Au electrodes without laser illumination, a constant current is formed and flows from electrode A to electrode B (meaning the drift electrons move from electrode B to electrode A); simultaneously, the interface band offset increases, resulting in an enhanced barrier height, as presented in Fig. 6c and d. Under both laser illumination and external bias voltage, the MoS_2 layer can be divided into two regions according to the diffusion direction of the separated electrons (left and right); the direction of the diffusion electrons is the same as that of the drift electrons in the left region, resulting in a large current and thus low resistance (called the conductivity increasing region), while the direction of the diffusion electrons is opposite to the direction of the drift electrons in the right region, leading to an increased resistance because of the enhanced scattering probability of carriers (called the conductivity decreasing region), as illustrated in Fig. 6e. It is supposed that the density of the drift electrons is $n_0(V)$ under a suitable bias voltage in the dark and the effective electron density can be simply determined by adding and subtracting the density of the drift and diffusion electrons under illumination of a laser beam, then the effective electron densities are $N(x) = n_0(V) + N_\lambda(x)$ and $N(x) = n_0(V) - N_\lambda(x)$ in the left and right regions, respectively. According to the relationship of conductivity (σ) and carrier density ($N(x)$), the resistivity ($\rho(x)$) can be expressed as:

$$\rho(x)=\begin{cases} \dfrac{1}{\left(n_0(V)+N_\lambda(0)\exp\left(-\dfrac{x-x_0}{l_0}\right)\right)q\mu_e} & (x_0\le x\le L)\\ \dfrac{1}{\left(n_0(V)-N_\lambda(0)\exp\left(-\dfrac{x_0-x}{l_0}\right)\right)q\mu_e} & (-L\le x<x_0)\end{cases} \quad (4)$$

where μ_e is the electron mobility, and q is the charge quantity. Then, the laser position-dependent photoresistance ($R(x_0)$) between electrode A and electrode B can be obtained from:

$$R(x_0)=\int_{-L}^{L}\rho(x)\mathrm{d}x/S \quad (5)$$

where S represents a constant cross-sectional area of the MoS_2 layer. Combining eqn (4) and (5) and solving the integration, the photoresistance can be deduced as follows:

$$\mathrm{R}(x_0)=\left(C+\frac{l_0}{n_0(V)q\mu_e}\ln\left(1-\frac{N_\lambda^2(0)}{n_0^2(V)}\exp\left(-\frac{2L}{l_0}\right)+\frac{N_\lambda(0)}{n_0(V)}\times\exp\left(-\frac{L-x_0}{l_0}\right)-\frac{N_\lambda(0)}{n_0(V)}\exp\left(-\frac{L+x_0}{l_0}\right)\right)\right)\Big/S \quad (6)$$

where $C=\dfrac{2L}{n_0(V)q\mu_e}-\dfrac{l_0}{n_0(V)q\mu_e}\ln\left(1-\dfrac{N_\lambda^2(0)}{n_0^2(V)}\right)$ is a constant coefficient. Generally, l_0 is supposed to be much larger than L, and $N_\lambda(0)$ is much smaller than $n_0(V)$ under illumination of a suitable laser power, thus eqn (6) can be simplified as:

$$R(x_0)\approx\left(C+\frac{2N_\lambda(0)}{n_0(V)^2q\mu_e l_0}\exp\left(\frac{-L}{l_0}\right)x_0\right)\Big/S \quad (7)$$

From eqn (7), it is clear that the resistance should decrease linearly with the laser beam (x_0) moving from $-L$ to L, which is in accordance with our results. However, under conditions of

This journal is © The Royal Society of Chemistry 2019

Published on 02 August 2019. Downloaded by Beijing Institute of Nanoenergy and Nanosystems CAS on 9/4/2019 3:00:41 PM.

very small bias voltages or sufficiently large laser power, $N_\lambda(0)$ should be comparable to or even larger than $n_0(V)$, so that the laser position-dependent resistance equation cannot be described by eqn (7), but rewritten as:

$$R(x_0) \approx \left(C + \frac{l_0}{n_0(V)q\mu_e}\ln\left(1 - \frac{N_\lambda{}^2(0)}{n_0{}^2(V)}\exp\left(-\frac{2L}{l_0}\right) + \frac{2N_\lambda(0)}{n_0(V)l_0}\exp\left(-\frac{L}{l_0}\right)x_0\right)\right)\Big/ S \quad (8)$$

The resistance begins to exhibit a nonlinear behavior when the laser power exceeds a certain value.

For the laser wavelength-dependent lateral photoresistance, it can also be well understood as $N_\lambda(0)$ is supposed to be related to both the wavelength and the quantum efficiency (ξ) under a certain laser power illumination, and the relationship can be expressed as $N_\lambda(0) \approx \frac{\xi P}{\hbar c}\lambda$, where P represents the illuminating power, $\hbar$ represents the Planck coefficient, and c represents the velocity of light. With the laser wavelength increasing from 405 to 671 nm, ξ should also improve gradually,[21,28] and then $N_\lambda(0)$ and the associated lateral photoresistance increase as a result of the combined effect of both λ and ξ. However, when the laser wavelength increases again from 671 to 980 nm, ξ starts to decrease largely, thus dominated mainly by ξ, and the lateral photoresistance decreases again (the difference of the best response wavelength between this heterostructure and the structure in ref. 21 may be attributed to the different qualities of the MoS_2 nanoplates due to various preparation methods).[28]

While for the gradually increased photoresistance (averaged) with increasing bias voltage, one possible reason is the enhanced scattering influence of the photoexcited electron–hole pairs as the number of the separated carriers improves with increasing external voltage because of the improved built-in field, as shown in Fig. 6f. Another possible reason is the heating effect (the surface conductivity of the MoS_2 layer exhibits a metal-like behavior due to lots of defect states). When the bias voltage is large enough, $N_\lambda(0)$ is supposed to be negligible as compared with $n_0(V)$, then eqn (6) can be approximately written as:

$$R(x_0) = \left(\frac{2L}{n_0(V)q\mu_e}\right)\Big/ S \quad (9)$$

The resistance shows an inherent value of the MoS_2 nanoplates and is independent of laser power again, which may be why the resistance remains nearly constant with laser position changing from A to B under very large bias voltages.

Finally, response speed, as another pivotal parameter of a photodetector, is also investigated in the heterojunction. Firstly, the time-dependent photoresistance response is measured under a 532 nm-laser illumination of 3 mW (laser position stays at x_0 = 0.225 mm) and a 0.2 V bias voltage with chopper frequency changing from 5 Hz to 50 Hz, with the results presented in Fig. 7a. Obviously, the photoresistance amplitude remains nearly constant between 5 Hz and 30 Hz, but seems to decrease slightly with increasing frequency again, suggesting that the response speed may limit the measurement frequency of ~30 Hz. Fig. 7b shows the extracted rise time (τ_{rise}) and the fall time (τ_{fall}). τ_{rise}(/τ_{fall}) decreases from 6.02 ms (/6.42 ms) to 5.17 ms (/5.86 ms) with the frequency increasing from 5 Hz to 30 Hz, and then decreases further to 5.13 ms (/5.82 ms) at 50 Hz. Then, the photoresistance response speed is also carefully studied under different voltages ranging from 0.2 V to 5.0 V, as shown in Fig. 7c. With increasing bias voltage, the photoresistance response decreases gradually, and the balanced photoresistance of laser on stage is the same as that of the LPR

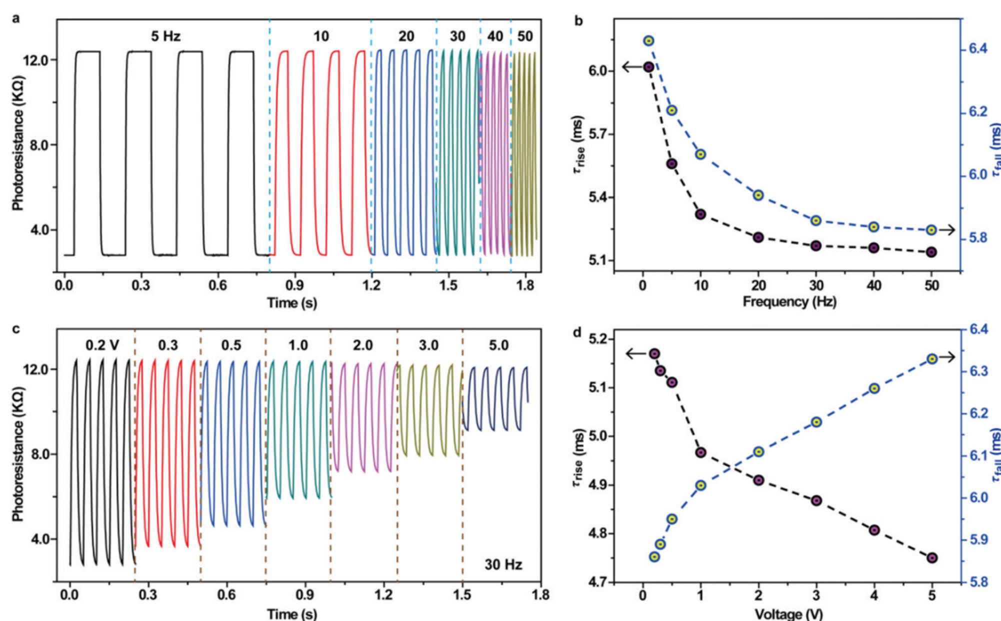

Fig. 7 (a) The R–t response of the PSD at different frequencies increasing from 5 Hz to 50 Hz. (b) The corresponding frequency-dependent rise and fall times. (c) The R–t response of the PSD with applying different bias voltages. (d) The corresponding voltage-dependent rise and fall times.

Published on 02 August 2019. Downloaded by Beijing Institute of Nanoenergy and Nanosystems CAS on 9/4/2019 3:00:41 PM.

results, indicating the stable response of the LPR performance. The bias voltage-dependent response times are given in Fig. 7d. τ_{rise}, which decreases slightly from 5.17 ms to 4.75 ms with external voltage increasing from 0.2 V to 5.0 V, exhibits completely contrary changing tendency to τ_{fall} (which increases a little from 5.86 ms to 6.33 ms). This can be ascribed to the enhanced interface barrier as the photo-generated carriers would be easily swept and quickly transmitted to the MoS_2 nanoplates and the Si substrate with increasing bias voltage during the laser on stage, respectively; meanwhile, the separated carriers would hardly jump back and get recombined during the laser off stage. This result demonstrates that a higher bias voltage can result in a faster rise time and a lower bias voltage can lead to a faster fall time to some extent.

4. Conclusions

In conclusion, a high quality MoS_2/Si p–n heterojunction has been successfully prepared by growing vertically standing MoS_2 nanoplates on the p-doped Si substrate by a magnetron sputtering technique. The MoS_2 layer shows a strong light absorption and a broadband spectral range (visible to near-infrared), and the heterojunction exhibits very high photoresponse characteristics. Based on the lateral photoelectric effect, this heterojunction is developed into a photovoltage, photocurrent and photoresistance-based multifunctional self-powered PSD. On account of the strong absorption, the quick intralayer transportation of the MoS_2 nanoplates, and the good quality of the heterojunction, the PSD shows unprecedented performance with voltage sensitivity as high as 391.1 mV mm^{-1}, current sensitivity as high as 285.2 μA mm^{-1}, resistance sensitivity as high as 21.61 KΩ mm^{-1}, excellent linearity (nonlinearity $<2\%$), and a very fast resistance response speed (4.75 ms/6.33 ms). More importantly, it is the first time that the LPRE is observed in the MoS_2/Si heterojunction. Although the LPR increases gradually with increasing laser power or decreasing bias voltage, there is a threshold power (or voltage), above (or below) which the laser position-dependent photoresistance curve tends to be nonlinear, and the threshold voltage increases with increasing laser power. Moreover, the response time can be effectively modulated by the bias voltage. Based on the scattering or transportation modulation theory of photo-generated carriers, these results can be successfully explained. Our work not only proposes a deep understanding of the LPRE in the MoS_2/Si heterojunction, but also offers an essential insight into the implementation of high-performance and novel photoelectric devices based on the photoresistance effect.

Conflicts of interest

They authors declare no competing financial interests.

Acknowledgements

This work is supported by the National Nature Science Foundation of China (Grant No. 11704094, 11504076, 51372064, 61405040, 51622205, 61675027, 51432005, and 61505010), the Nature Science Foundation of Hebei Province (Grant No. F2019201047, F2018201198, F2017201141, and E2017201227), the Science and Technology Research project of Hebei Province Higher Education Institution (Grant No. ZD2016036), Nature Science Foundation for Distinguished Young Scholars of Hebei University (Grant No. 2015JQ03), the Young Talents of Hebei Province, the Support of National Key R & D project from Minister of Science and Technology, China (2016YFA0202703), and the "Thousand Talents" program of China for pioneering researchers and innovative teams.

Notes and references

1 Q. H. Wang, K. K. Zadeh, A. Kis, J. N. Coleman and M. S. Strano, *Nat. Nanotechnol.*, 2012, **7**, 699.
2 D. Jariwala, V. K. Sangwan, L. J. Lauhon, T. J. Marks and M. C. Hersam, *ACS Nano*, 2014, **8**, 1102–1120.
3 K. F. Mak and J. Shan, *Nat. Photonics*, 2016, **10**, 216–226.
4 W. Z. Wu, L. Wang, Y. L. Li, F. Zhang, L. Lin, S. M. Niu, D. Chenet, X. Zhang, Y. F. Hao, T. F. Heinz, J. Hone and Z. L. Wang, *Nature*, 2014, **514**, 470–474.
5 A. K. Geim and I. V. Grigorieva, *Nature*, 2013, **499**, 419–425.
6 M. L. Tsai, S. H. Su, J. K. Chang, D. S. Tsai, C. H. Chen, C. Wu, L. J. Li, L. J. Chen and J. H. He, *ACS Nano*, 2014, **8**, 8317–8322.
7 B. Radisavljevic, A. Radenovic, J. Brivio, V. Giacometti and A. Kis, *Nat. Nanotechnol.*, 2011, **6**, 147.
8 M. Bernardi, M. Palummo and J. C. Grossman, *Nano Lett.*, 2013, **13**, 3664–3670.
9 K. F. Mak, C. Lee, J. Hone, J. Shan and T. F. Heinz, *Phys. Rev. Lett.*, 2010, **105**, 136805.
10 D. S. Tsai, K. K. Liu, D. H. Lien, M. L. Tsai, C. F. Kang, C. A. Lin, L. J. Li and J. H. He, *ACS Nano*, 2013, **7**, 3905.
11 D. J. Late, B. Liu, H. S. S. R. Matte, V. P. Dravid and C. N. R. Rao, *ACS Nano*, 2012, **6**, 5635–5641.
12 Z. Y. Yin, H. Li, H. Li, L. Jiang, Y. M. Shi, Y. H. Sun, G. Lu, Q. Zhang, X. D. Chen and H. Zhang, *ACS Nano*, 2012, **6**, 74–80.
13 W. Choi, M. Y. Cho, A. Konar, J. H. Lee, G. B. Cha, S. C. Hong, S. Kim, J. Kim, D. Jena, J. Joo and S. Kim, *Adv. Mater.*, 2012, **24**, 5832–5836.
14 Q. J. Xiang, J. G. Yu and M. Jaroniec, *J. Am. Chem. Soc.*, 2012, **134**, 6575–6578.
15 W. J. Zhou, Z. Y. Yin, Y. P. Du, X. Huang, Z. Y. Zeng, Z. X. Fan, H. Liu, J. Y. Wang and H. Zhang, *Small*, 2013, **9**, 140–147.
16 H. Li, Z. Y. Yin, Q. Y. He, X. Huang, G. Lu, D. W. H. Fam, A. L. Y. Tok, Q. Zhang and H. Zhang, *Small*, 2012, **8**, 63–67.
17 Q. Y. He, Z. Y. Zeng, Z. Y. Yin, H. Li, S. X. Wu, X. Huang and H. Zhang, *Small*, 2012, **8**, 2994–2999.
18 S. Wi, H. Kim, M. Chen, H. Nam, L. J. Guo, E. Meyhofer and X. G. Liang, *ACS Nano*, 2014, **8**, 5270–5281.
19 D. Kufer, I. Nikitskiy, T. Lasanta, G. Navickaite, F. H. L. Koppens and G. Konstantatos, *Adv. Mater.*, 2015, **27**, 176–180.
20 Z. J. Xu, S. S. Lin, X. Q. Li, S. J. Zhang, Z. Q. Wu, W. L. Xu, Y. H. Lu and S. Xu, *Nano Energy*, 2016, **23**, 89–96.

This journal is © The Royal Society of Chemistry 2019

Published on 02 August 2019. Downloaded by Beijing Institute of Nanoenergy and Nanosystems CAS on 9/4/2019 3:00:41 PM.

21 R. D. Cong, S. Qiao, J. H. Liu, J. S. Mi, W. Yu, B. L. Liang, G. S. Fu, C. F. Pan and S. F. Wang, *Adv. Sci.*, 2018, **5**, 1700502.
22 E. Singh, K. S. Kim, G. Y. Yeom and H. S. Nalwa, *ACS Appl. Mater. Interfaces*, 2017, **9**, 3223–3245.
23 X. D. Wang, P. Wang, J. L. Wang, W. D. Hu, X. H. Zhou, N. Guo, H. Huang, S. Sun, H. Shen, T. Lin, M. H. Tang, L. Liao, A. Q. Jiang, J. L. Sun, X. J. Meng, X. S. Chen, W. Lu and J. H. Chu, *Adv. Mater.*, 2015, **27**, 6575–6581.
24 J. S. Miao, W. D. Hu, Y. L. Jing, W. J. Luo, L. Liao, A. L. Pan, S. W. Wu, J. X. Cheng, X. S. Chen and W. Lu, *Small*, 2015, **11**, 2392–2398.
25 T. Mueller, F. N. Xia and P. Avouris, *Nat. Photonics*, 2010, **4**, 297–301.
26 M. Engel, M. Steiner and P. Avouris, *Nano Lett.*, 2014, **14**, 6414–6417.
27 D. Z. Zhang, Y. E. Sun, P. Li and Y. Zhang, *ACS Appl. Mater. Interfaces*, 2016, **8**, 14142–14149.
28 S. Qiao, B. Zhang, K. Y. Feng, R. D. Cong, W. Yu, G. S. Fu and S. F. Wang, *ACS Appl. Mater. Interfaces*, 2017, **9**, 18377–18387.
29 Z. L. Wang, *Adv. Funct. Mater.*, 2008, **18**, 3553–3567.
30 R. Cheng, D. H. Li, H. L. Zhou, C. Wang, A. X. Yin, S. Jiang, Y. Liu, Y. Chen, Y. Huang and X. F. Duan, *Nano Lett.*, 2014, **14**, 5590–5597.
31 T. Roy, M. Tosun, X. Cao, H. Fang, D. H. Lien, P. Zhao, Y. Z. Chen, Y. L. Chueh, J. Guo and A. Javey, *ACS Nano*, 2015, **9**, 2071–2079.
32 P. P. Wang, H. Y. Sun, Y. J. Ji, W. H. Li and X. Wang, *Adv. Mater.*, 2014, **26**, 964–969.
33 Y. D. Liu, J. M. Guo, A. F. Yu, Y. Zhang, J. Z. Kou, K. Zhang, R. M. Wen, Y. Zhang, J. Y. Zhai and Z. L. Wang, *Adv. Mater.*, 2018, **30**, 1704524.
34 F. Xue, L. B. Chen, J. Chen, J. B. Liu, L. F. Wang, M. X. Chen, Y. K. Pang, X. N. Yang, G. Y. Gao, J. Y. Zhai and Z. L. Wang, *Adv. Mater.*, 2016, **28**, 3391–3398.
35 L. Wang, J. S. Jie, Z. B. Shao, Q. Zhang, X. H. Zhang, Y. M. Wang, Z. Sun and S. T. Lee, *Adv. Funct. Mater.*, 2015, **25**, 2910–2919.
36 S. Qiao, R. D. Cong, J. H. Liu, B. L. Liang, G. S. Fu, W. Yu, K. L. Ren, S. F. Wang and C. F. Pan, *J. Mater. Chem. C*, 2018, **6**, 3233–3239.
37 M. K. Wu, J. R. Ashburn and C. J. Torng, *Phys. Rev. Lett.*, 1987, **58**, 908–910.
38 M. N. Baibich, J. M. Broto, A. Fert, F. N. V. Dau and F. Petroff, *Phys. Rev. Lett.*, 1988, **61**, 2472–2475.
39 B. Polyakov, B. Daly, J. Prikulis, V. Lisauskas, B. Vengalis, M. A. Morris, J. D. Holmes and D. Erts, *Adv. Mater.*, 2006, **18**, 1812–1816.
40 C. Q. Yu and H. Wang, *Adv. Mater.*, 2010, **22**, 966–970.
41 X. Q. Xie, Z. M. Ao, D. W. Su, J. Q. Zhang and G. X. Wang, *Adv. Funct. Mater.*, 2015, **25**, 1393–1403.
42 H. Li, Q. Zhang, C. C. R. Yap, B. K. Tay, T. H. T. Edwin, A. Olivier and D. Baillargeat, *Adv. Funct. Mater.*, 2012, **22**, 1385–1390.
43 R. Martins and E. Fortunato, *Rev. Sci. Instrum.*, 1995, **66**, 2927.
44 J. Henry and J. Livingstone, *Adv. Mater.*, 2001, **13**, 1023.
45 E. Fortunato, G. Lavareda, R. Martins, F. Soares and L. Fernandes, *Sens. Actuators, A*, 1996, **51**, 135.
46 C. Q. Yu, H. Wang, S. Q. Xiao and Y. X. Xia, *Opt. Express*, 2009, **17**, 21712.
47 S. Qiao, Y. N. Liu, J. H. Liu, J. H. Chen, S. F. Wang and G. S. Fu, *IEEE Electron Device Lett.*, 2016, **37**, 201.
48 K. J. Jin and K. Zhao, *Appl. Phys. Lett.*, 2007, **91**, 081906.
49 C. Q. Yu, H. Wang and Y. X. Xia, *Appl. Phys. Lett.*, 2009, **95**, 263506.
50 S. Qiao, K. Y. Feng, Z. Q. Li, G. S. Fu and S. F. Wang, *J. Mater. Chem. C*, 2017, **5**, 4915.
51 W. H. Wang, Z. Z. Yan, J. F. Zhang, J. P. Lu, H. Qin and Z. H. Ni, *Optica*, 2018, **5**, 27–31.